Molecules and Cells

Research Article

Targeting of CYP2E1 by miRNAs in alcohol-induced intestine injury

Hyejin Mun[1,2,16], Sungyul Lee[3,16], Suyoung Choi[4,5,6,16], Ji-Hoon Jeong[2], Seungbeom Ko[1], Yoo Lim Chun[1,7], Benjamin Deaton[1], Clay T. Yeager[1], Audrey Boyette[1], Juliana Palmera[1], London Newman[1], Ping Zhou[8,9], Soona Shin[8,9], Dong-Chan Kim[10], Cari A. Sagum[11], Mark T. Bedford[11], Young-Kook Kim[12], Jaeyul Kwon[4,5,6,13,14], Junyang Jung[7,*], Jeong Ho Chang[15,*], and Je-Hyun Yoon[1,2,*]

[1]Department of Biochemistry and Molecular Biology, Medical University of South Carolina, Charleston, SC 29425, USA, [2]Department of Oncology Science, University of Oklahoma, Oklahoma City, OK 73104, USA, [3]School of Biological Sciences, Seoul National University, Seoul 08826, Republic of Korea, [4]Department of Infection Biology, College of Medicine, Chungnam National University, Daejeon 35015, Republic of Korea, [5]Department of Medical Science, College of Medicine, Chungnam National University, Daejeon 35015, Republic of Korea, [6]Brain Korea 21 FOUR Project for Medical Science, Chungnam National University, Daejeon 35015, Republic of Korea, [7]Department of Anatomy and Neurobiology, College of Medicine, Kyung Hee University, 26, Kyungheedae-ro, Dongdaemun-gu, Seoul 02447, Republic of Korea, [8]Division of Pediatric General and Thoracic Surgery, Cincinnati Children's Hospital Medical Center, Cincinnati, OH 45229, USA, [9]Department of Surgery, University of Cincinnati College of Medicine, Cincinnati, OH 45267, USA, [10]Division of Medical Device R&D Center, NQ-Lab, Inc.,Yongin-si, Gyeonggi-do 16827, Republic of Korea, [11]Department of Epigenetics and Molecular Carcinogenesis, The University of Texas MD, Anderson Cancer Center, Houston, TX 77030, USA, [12]Department of Biochemistry, Chonnam National University Medical School, Hwasun 58128, Republic of Korea, [13]Department of Medical Education, College of Medicine, Chungnam National University, Daejeon 35015, Republic of Korea, [14]Translational Immunology Institute, Chungnam National University, Daejeon 35015, Republic of Korea, [15]Department of Biology Education, Kyungpook National University, Daegu 41566, Republic of Korea

*Correspondence:jjung@khu.ac.kr (J.J.); jhcbio@knu.ac.kr (J.H.C.); ehyun-yoon@ouhsc.edu (J.-H.Y.).
https://doi.org/10.1016/j.mocell.2024.100074

ABSTRACT

Although binge alcohol-induced gut leakage has been studied extensively in the context of reactive oxygen species–mediated signaling, it was recently revealed that post-transcriptional regulation plays an essential role as well. Ethanol (EtOH)-inducible cytochrome P450-2E1 (CYP2E1), a key enzyme in EtOH metabolism, promotes alcohol-induced hepatic steatosis and inflammatory liver disease, at least in part by mediating changes in intestinal permeability. For instance, gut leakage and elevated intestinal permeability to endotoxins have been shown to be regulated by enhancing CYP2E1 mRNA and CYP2E1 protein levels. Although it is understood that EtOH promotes CYP2E1 induction and activation, the mechanisms that regulate CYP2E1 expression in the context of intestinal damage remain poorly defined. Specific miRNAs, including miR-132, miR-212, miR-378, and miR-552, have been shown to repress the expression of CYP2E1, suggesting that these miRNAs contribute to EtOH-induced intestinal injury. Here, we have shown that CYP2E1 expression is regulated post-transcriptionally through miRNA-mediated degradation, as follows: (1) the RNA-binding protein AU-binding factor 1 (AUF1) binds mature miRNAs, including CYP2E1-targeting miRNAs, and this binding modulates the degradation of corresponding target mRNAs upon EtOH treatment; (2) the serine/threonine kinase mammalian Ste20-like kinase 1 (MST1) mediates oxidative stress-induced phosphorylation of AUF1. Those findings suggest that reactive oxygen species–mediated signaling modulates AUF1/miRNA interaction through MST1-mediated phosphorylation. Thus, our study demonstrates the critical functions of AUF1 phosphorylation by MST1 in the decay of miRNAs targeting CYP2E1, the stabilization of CYP2E1 mRNA in the presence of EtOH, and the relationship of this pathway to subsequent intestinal injury.

Keywords: AU-binding factor 1, Cytochrome P450-2E1, Intestine, microRNA, Mammalian Ste20-like kinase 1

[16] Co-first authors.

eISSN: 1016-8478

INTRODUCTION

Alcohol use disorder (AUD) occurs in 20 million Americans and costs our nation $225 billion a year (Sacks et al., 2015). From 2006-2010, excessive drinking was responsible for 1 in 10 deaths among working adults aged 20-64 years. During that same period, excessive alcohol use in the United States led to approximately 88,000 deaths, shortening the lives of those who died by an average of 30 years for a total of 2.5 million years of potential life lost (Stahre et al., 2014; Yoon, 2010). The most severe and costly medical problems associated with AUD are intestinal and liver disease, and a high percentage of chronic heavy alcohol users develop various digestive disorders. It is generally accepted that the negative impacts of alcohol are produced by components of the normal flora that act as pathogens when they invade nongut tissue from the intestine, traveling through the venous portal system to the liver where they either act on the organ directly or indirectly by inducing hepatic inflammation (Reuben, 2008; Sheron, 2016)

The mechanisms by which alcohol disrupts the intestinal barrier and increases gut permeability, subsequently allowing penetration of pathogens ("alcohol-induced gut leakage") have been well-characterized. One of the most critical proteins in this process is cytochrome P450-2E1 (CYP2E1), a metabolic enzyme that converts ethanol (EtOH) to acetaldehyde, generates reactive oxygen species (ROS), and promotes intestinal cell death via the c-Jun N-terminal kinases signaling pathway (Abdelmegeed et al., 2013). Global knockout of CYP2E1 in mice suppresses alcohol-induced multiorgan injury, including in the gut, liver, kidney, and brain. Although chronic exposure to alcohol decreases CYP2E1 levels in the intestine, CYP2E1 levels can be immediately raised through acute alcohol exposure in the form of binge drinking, a pattern of drinking that brings a blood alcohol concentration to 0.08 g percent or above. The alcohol-related regulation of CYP2E1 occurs at multiple levels that include rapid degradation pathways, release from the intestine, and post-transcriptional silencing (Cho et al., 2017). While specific miRNAs that repress expression of *CYP2E1* transcripts have previously been described (Miao et al., 2016; Mohri et al., 2010; Shukla et al., 2013), the involvement of these miRNAs in binge alcohol-induced gut leakage has not been investigated (Natarajan et al., 2015).

We discovered that *CYP2E1*-targeting miRNAs are downregulated in response to binge alcohol-induced phosphorylation of AU-binding factor 1 (AUF1) and that AUF1 phosphorylation is mediated by the mammalian Ste20-like kinase 1 (MST1) Ser/Thr kinase. These observations are both novel and of potential significance because they support the idea that the MST1-AUF1-miRNA-CYP2E1 pathway plays an integral role in regulating the gastrointestinal response to binge alcohol exposure (Newton et al., 1995).

MATERIALS AND METHODS

Mice

The *MST1* knockout mice were generated by crossing $MST1^{-/-}$Mst2$^{-/-}$ mice from Jackson Laboratory (Stock No: 017635). $MST1^{+/+}$ and $^{-/-}$ mice were utilized for a model of binge EtOH-induced gut injury approved by the National Institutes of Health/National Institute on Aging (Bertola et al., 2013). The mice were fed a control diet (Lieber-DeCarli diet *ad libitum*) for 5 days to acclimate them to a liquid diet and tube feeding. After 5 days, EtOH-fed groups were allowed *ad libitum* access to the Lieber-DeCarli diet containing 5% EtOH (vol/vol) for 10 days. Control groups were pair-fed with an isocaloric control diet. On the morning of day 11, the mice were provided a single dose of EtOH (5 g/kg body weight) or isocaloric maltose dextrin by oral gavage. After 9 h, the mice were sacrificed for RNA, protein, and tissue from the intestine, liver, and brain. For a model of binge EtOH-induced gut injury in rat, we followed a protocol as published previously (Banerjee et al., 2015). All animal experiments were approved by, and adhered to the guidelines of, the Medical University of South Carolina Animal Care and Use Committee.

Intestine Crypt Organoid Culture

Intestine crypt organoids were cultured as described previously (Devall et al., 2020; Forsyth et al., 2010; Lu et al., 2017; Suh et al., 2017). Briefly, intestine crypts were digested with Accumax (Stem cell technology) for 5 min and separated through cell strainers (70 μm and then 40 μm) for single-cell collection. The resulting cells were suspended in Matrigel with a reduced amount of growth factor (Corning 356231) for polymerization. The culture media were applied with 50% conditioned medium from L-WRN cells (ATCC CRL-3276) and 50% Advanced DMDM/F12 containing 1 mM *N*-acetyl cysteine, B27 supplement, N2 supplement, 50 ng/mL mouse EGF, and 10 μM Y-27632.

Human Intestinal Cell Culture and Transfection

T84 cell lines were obtained from ATCC and HIEC-6 (ATCC CCL-248 and CRL-3266) and cultured in Dulbecco's Modified Eagle Medium supplemented with 10% fetal bovine serum and penicillin/streptomycin. Mouse MST1 cDNA plasmid was provided by Dr Eui-Ju Choi of Korea University, Korea (Yun et al., 2011) and transfected into T84, HIEC-6 using lipofectamine. Synthetic miRNAs mimicking miR-132, 212, 378, and 552 were purchased from ThermoFisher Scientific (mirVana miRNA mimics). We have used 3 to 10 nM concentration for transfection to T84, HIEC-6 cells by using Lipofectamine RNAiMAX for 48 h.

Sodium Dodecyl Sulfate Gel Electrophoresis and Western Blot Analysis

Whole-cell lysates, prepared in radioimmunoprecipitation assay buffer, were separated by sodium dodecyl sulfate-polyacrylamide gel electrophoresis and transferred onto nitrocellulose membranes (Invitrogen iBlot Stack). Immunoblots were performed using antibodies against CYP2E1 (1:1000, Abcam ab28146), TUBA (1:5000, SCBT sc-5286), MST1 (1:1000, CST #3682), p-MST1 (1:500, CST #49332), AUF1 (1:2000, Millipore 07-260), HuR (1:2000, SCBT sc-5261), QKI (1:1000, Abcam ab126742), HA (1:5000, Sigma 11867423001), and Actin (1:5000, SCBT sc-47778). Horseradish-peroxidase–conjugated secondary antibodies were purchased from GE Healthcare. A rabbit polyclonal phosphor-threonine 127 AUF1 antibody was produced by injection of a synthetic peptide (CEVVDCT(p)LKLDPIT) and affinity purification (Applied Biological Materials Inc.).

Immunohistochemistry and Immunofluorescence Assay

Immunostaining was performed as described previously (Lee et al., 2018). Briefly, formalin-fixed paraffin-embedded tissue sections were subjected to deparaffinizing, rehydrating, and antigen retrieval. For chromogenic immunohistochemistry, sections were stained per the manufacturer's protocol (VECTASTAIN Elite ABC-Horseradish Peroxidase Kit, Peroxidase, PK-6106, Vector Laboratories), and hematoxylin was used for nuclear counterstain. For immunofluorescence, 4′,6-diamidino-2-phenylindole was used for nuclear counterstain. Antibodies: AUF1 (1:500 for immunohistochemistry, 1:1000 for immunofluorescence, 07-260 Millipore); epithelial markers epithelial cell adhesion molecule (EPCAM) (1:50, ab71916 Abcam); hepatocyte nuclear factor 4 alpha (1:100, PP-H1415-00 R&D); LGR5 (1:500, ab273092 Abcam).

RNA Immunoprecipitation

RNA immunoprecipitation (RIP) analysis from whole-cell extracts was performed as described previously (Min et al., 2017a, 2017b) Briefly, cells were lyzed in a buffer containing 20 mM Tris-HCl (pH 7.5), 100 mM KCl, 5 mM $MgCl_2$, and 0.5% NP-40, then cleared by centrifugation. The lysates were incubated with protein A-Sepharose beads coated with antibodies against AUF1 (Millipore 07-260) with control IgG (SCBT) at 4°C for 1 h. After the beads were washed 4 times with NT2 buffer [50 mM Tris-HCl (pH 7.5), 150 mM NaCl, 1 mM $MgCl_2$, 0.05% NP-40], the immunoprecipitates were treated with 20 units of RNase-free DNase I at 37°C for 15 min and proteinase K (0.5 mg/mL) in 0.1% sodium dodecyl sulfate at 55°C for 15 min to remove DNAs and proteins, respectively. The RNAs isolated from the immunoprecipitations by acidic phenol extraction were then subjected to RT-qPCR using the primers listed in Supplementary Table 1. The RIP results were normalized to *Gapdh* mRNA or *U6* RNA.

Real-Time RT-qPCR

Total RNA was isolated with Trizol reagent (Invitrogen) and reverse transcribed with the Maxima reverse transcriptase (Fermentas). Expression of specific mRNAs was determined with iCycler (Bio-Rad) using the KAPA SYBR FAST qPCR kit (Kapa Biosystems). MicroRNA quantification was performed after RNA extraction from immunoprecipitated samples (with anti-AUF1 or control IgG), polyadenylation (System Biosciences QuantiMiR kit), and hybridization with oligo-dT adaptors. After reverse transcription, cDNAs were quantified by qPCR with microRNA-specific primers or with primers to detect the control transcript *U6* along with a universal primer. All the sources of qPCR primers used in the study are listed in Supplementary Table 1.

Cumulative Distribution Fraction Analysis

Cumulative distribution analysis of mRNA $\log_2$ fold changes expression was performed in R. For each group of interest, the empirical cumulative distribution functions of $\log_2$ fold mRNA expression values were computed using the ecdf function, and pairs of curves to be compared were displayed with plot.cdf. A significant difference between the cumulative distribution curves was determined using the Kolmogorov-Smirnov test, and the corresponding *P* values were included in the plot.

Total RNA Sequencing Analysis

Total RNA was isolated using TRIzol according to the manufacturer's instructions. For high throughput RNA sequencing, we followed the standard protocol of Illumina sequencing, using the TruSeq Stranded Total RNA kit with Ribo-Zero (Part#15031048 Rev. E) and NovaSeq6000 S4 (150 bp PE). Analyses were performed on 2 paired-ends samples. Trimmed reads are mapped to reference genome for MM9 with HISAT2. After the read mapping, Stringtie was utilized for transcript assembly. The expression profile was calculated for each sample and transcript/gene as a read count and Fragment per Kilobase of transcript per Million mapped reads (Supplementary Table 2). The raw data have been deposited to GEO GSE206348.

miRNA Sequencing Analysis

Briefly, in a total reaction volume of 20 μL, 2 μg of total RNA were ligated to 100 pmol adenylated 3′ adapter containing a unique pentamer barcode (App (Barcode) TCGTATGCCGTCTTCTGCTTGT), and 1 μg of Rnl2 (1-249) K227Q (the plasmid for expression of recombinant ligase is available at www.addgene.org) in 50 mM Tris-HCl, pH 7.6, 10 mM $MgCl_2$, 10 mM 2-mercaptoethanol, 0.1 mg/mL acetylated bovine serum albumin (Sigma), and 15% dimethyl sulfoxide for 16 h on ice. Following 3′ adapter ligation, the barcoded samples were pooled, and products were purified on a 15% denaturing polyacrylamide gel. Small RNAs measuring 45 to 50 nt in length were excised from the gel, then eluted and ligated to 100 pmol 5′ oligoribonucleotide adapter (GUUCAGAGUUCUACAGUCCGACGAUC) in a 20 μL reaction volume using 1 μg of T4 RNA ligase 1 (ThermoFisher) in 50 mM Tris-HCl, pH 7.6, 10 mM $MgCl_2$, 10 mM 2-mercaptoethanol, 0.1 mg/mL acetylated bovine serum albumin, 0.2 mM adenosine triphosphate, and 15% dimethyl sulfoxide for 1 h at 37°C. Ligated small RNAs were purified on a 12% polyacrylamide gel, reverse transcribed using SuperScript III Reverse Transcriptase (Life Technologies), and amplified by PCR using appropriate primers (forward primer: AATGATACGGCGACCACCGACAGGTTCAGAGTTCTACAGTCCGA; reverse primer: CAAGCAGAAGACGGCATACGA). cDNA libraries were sequenced on an Illumina HiSeq 2000 instrument at the Rockefeller University Genomics Resource Center.

Circular RNA Analysis

Profiling of mouse circular RNA junctions (GSE206348) was performed as described previously (Kim, 2019). The raw data of total RNA-seq were filtered using the Trimmomatic trimmer tool to eliminate the 5′ and 3′ adaptor sequences (Bolger et al., 2014). The resulting sequences were aligned to the mouse Reference Sequence (mm10) using the STAR aligner. FKPM of the junction sequences was calculated using the DCC algorithm (Cheng et al., 2016).

Single-Cell RNA Sequencing Matrix Data Analysis

The single-cell RNA sequencing data generated from the colon of a female C57BL/6J mouse was downloaded from the NCBI Gene Expression Omnibus database (Parigi et al., 2022) (GEO; accession number GSE163638) as a count matrix. The barcodes, features, and matrix dataset were processed, explored, and visualized using the Cellenics community instance (https://scp.biomage.net/) hosted by Biomage (https://biomage.net/). In brief, the matrix

dataset, dextran sodium sulfate–treated group, was excluded from the raw data. Cells that did not meet certain quality criteria, including the use of the classifier filter, checking cell size distribution (less than 200 unique molecular identifiers), assessing mitochondrial content (over 15%), evaluating the number of genes vs unique molecular identifiers and doublet filter within cells. Next, the filtered dataset was embedded into a Uniform Manifold Approximation and Projection graph. Clusters were identified using Louvain graph-based clustering, and the cell type annotation for each cluster was determined using scType function in Cellenics. The cell clusters were annotated base on the known marker gene expression. Concretely, we utilized the following marker genes for cell type annotation: EPCAM for intestinal epithelial cells; Thy1, Vim, and Col1a2 for fibroblast; Hand2 and Tubb2b for neural/glial cells; Tagln, Foxf1, and vim for myofibroblast; Kcnj8 and Abcc9 for pericyte; Ptprc for myeloid cells (Kwon et al., 2021). Also, we utilized for subset analysis in intestinal epithelial cells: Lgr5, Ascl2, Alcam, and Lrig1 for intestinal stem cells; Vil1, and Anpep for enterocytes; Lyz for Paneth cells; Chga for goblet cells (Yeung et al., 2011). The average mRNA expression value was exported from Cellenics and generated using GraphPad Prism 8 (Prism 8, GraphPad).

Mass Spectrometry

The active MST1 (0.5 μg, Merk Millipore) was incubated for 30 min at 37°C with recombinant human AUF1 p37 (2 μg) and 0.25 mM ATP in 20 μL of a kinase reaction buffer, the reaction mixtures were processed with the filter assisted sample preparation method (Wepf et al., 2009). In brief, the protein samples were dissolved in 9 M urea and subjected to reduction with 5 mM tris(2-carboxyethyl) phosphine (Sigma) at 60°C for 45 min and to alkylation with 20 mM C_2H_4INO (Sigma) at 25°C for 15 min. The samples were then cleaned 3 times with a 30-kDa Amicon Filter (UFC503096, Millipore), with 9 M urea and twice with 30 mM NH_4HCO_3. After proteolysis with trypsin (Promega) and chymotrypsin (Roche) at a 1:20 ratio for 12 h at 37°C, the digested peptides were desalted and eluted with 0.1% trifluoroacetic acid in 60% acetonitrile. The extracted peptides were dried and then resuspended in 7 μL of 0.1% formic acid for liquid Chromatography with tandem mass spectrometry, performed with an LTQ-Orbitrap Velos instrument (ThermoFisher Scientific) interfaced with a nanoLC-2D and nanoACQUITY UltraPerformance LC system (Waters). Precursor and fragment ions were analyzed at a resolution of 30,000 and 7,500, respectively. Peptide sequences were identified from isotopically resolved masses in MS and MS/MS spectra extracted with and without deconvolution with the use of Thermo Scientific Xtract software. The data were analyzed with Proteome Discoverer 1.3 software (Thermo Scientific) configured with Mascot and Sequest search nodes and were searched against Refseq version 46 human entries with oxidation on Met, deamidation of Asn and Gln, and phosphorylation of Ser, Thr, or Tyr as variable modifications and carbamidomethylation of Cys as a fixed modification. Tolerances for precursor and fragment masses were set to 15 ppm and 0.03 Da, respectively. A peptide validator node was used for peptide confirmation, and a 1% false discovery rate cutoff was used to filter the data.

Human RNA-Binding Domain Array Analysis

This assay was performed according to modifications of a previously described method (Chen et al., 2020). Glutathione S-transferase (GST) recombinant proteins were designed to include reported and suspected RNA-binding domains and synthesized with Biomatik Corporation in the pGEX-4T1 vector. Recombinant proteins were expressed and purified using GST-fusion system. GST proteins were then arrayed, in duplicate, using an Aushon 2470 Microarrayer (Quanterix) onto nitrocellulose-coated glass slides (Grace Bio-Labs). The RNA-Binding Domains Array contains approximately 354 GST recombinant proteins, which include SAF-A/B, Acinus and PIAS, RNA recognition motif (RRM), K homology, Double-stranded RNA binding motif, and YT521-B homology domains. Full-length GST and Histidine fusion proteins were printed, in duplicate, onto nitrocellulose-coated glass slides.

To screen for potential RNA-protein interactions, the RNA-Binding Domains Array was probed with biotinylated-miRNA oligonucleotides. miRNA oligonucleotides were designed with 5′ biotinylation and 3′ Cy5 fluorophore and synthesized by Integrated DNA Technologies. Microarrays were blocked for 1 h with RNA-binding buffer (20 mM Tris-HCl at pH 7.4, 200 mM KCl, 0.2 mM ethylenediaminetetraacetic acid, 0.05% NP-40, 2 μg/μL heparin). miRNA oligonucleotides were prepared for microarray probing by incubating miRNA at 1 μM with streptavidin-Cy3 in RNA-binding buffer in the presence of 0.4 U RNase inhibitor. Primed miRNA oligonucleotides were then incubated with microarrays overnight at 4°C in RNA-binding buffer with RNase inhibitor. Microarrays were dried and scanned using the InnoScan 1100 AL Fluorescence Scanner (Innopsys) and intensities were quantified using Mapix software.

Structure Modeling of AUF1 and miRNA Fragments

To prepare an AUF1 model containing RRM1 and RRM2, the crystal structure of AUF1-RRM1 (Pdb code, 5IM0) and the nuclear magnetic resonance structure of AUF1-RRM2-Telomeric DNA (TAGG) complex (Pdb code, 1WTB) were combined based on the crystal structure of HuR (RRM1+RRM2) in complex with c-fos mRNA (Pdb code, 4ED5) (Choi et al., 2016; Enokizono et al., 2005; Wang et al., 2013). Separate molecular dockings with the AUF1 model and each of miR-132, miR-212, and miR-378 were carried out by PyRx Virtual Screening Tool Autodock Vina Version 0.9.7, at every 6 bp-RNA fragment 5 times per model, followed by a determination of the minimum binding energy reflected among 15 calculated values (Trott and Olson, 2010). For running the software, the Protein Data Bank (PDB) file was converted to PDBQT format via OpenBabelGUI program (O'Boyle et al., 2011). The docking models were presented by PyMOL software (The PyMOL Molecular Graphics System, Version 2.0 Schrödinger, LLC.).

Quantification and Statistical Analysis

Data are expressed as the mean ± SD of the values from at least 3 independent experiments performed, as indicated in the corresponding figure legends. The numbers of biological replicates, and what they represent, are indicated in each figure legend. Two-tailed Student's *t* tests were used for single comparison, and *P* values below .05 were considered statistically significant.

RESULTS

CYP2E1 Is Essential for EtOH-Induced Intestine Injury

To test our hypothesis, we initially established cell culture and *in vivo* models of intestinal injury. First, we isolated crypts from the

small intestine of mice and dissociated them into single cells. We generated organoids from the isolated crypt cells in either the presence or absence of EtOH (50 mM) in a medium containing Wnt, R-spondin, and noggin (WNR) (Miyoshi and Stappenbeck, 2013). We also treated the organoids with a CYP2E1 inhibitor, chlormethiazole (Chen et al., 2014; Gebhardt et al., 1997; Stresser et al., 2016), to determine whether CYP2E1 was critical for the formation of intestinal organoids. As shown in Figure 1, intestinal organoids form within 5 to 8 days under these growth conditions, and their formation is

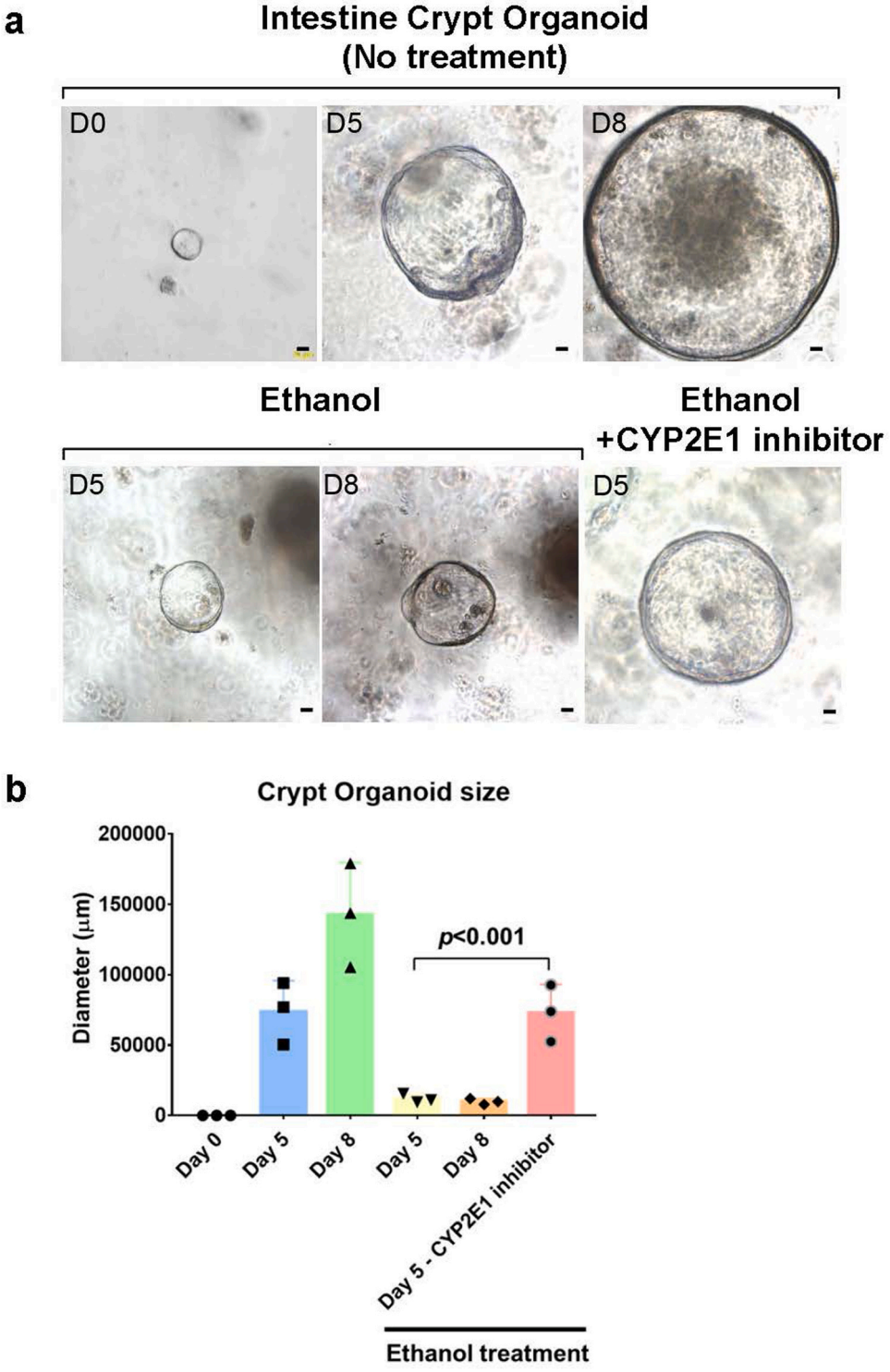

Fig. 1. CYP2E1 mediates ethanol-induced repression of intestinal crypt cell organoid formation. (a) Measurements of intestinal crypt organoid size, with or without EtOH treatment, and in the presence or absence of a CYP2E1 inhibitor, chlormethiazole. (b) Quantitation of crypt organoid size in the presence or absence of ethanol or CYP2E1 inhibitor. The graphs are the average of 3 independent experiments with standard deviation.

suppressed upon EtOH treatment. Moreover, cotreatment with the CYP2E1 inhibitor suppresses the inhibitory effect of EtOH on organoid formation (Fig. 1a and b). These results support the idea that EtOH's inhibitory effects on intestinal organoid formation are mediated by CYP2E1.

Steady-State Levels of miRNAs and mRNAs Fluctuate in Intestine From EtOH-Fed Mice

Next, we established a mouse model approved by the National Institutes of Health/National Institute on Aging (Bertola et al., 2013) to study binge alcohol-induced gut injury *in vivo* (Fig. 2a). In this model, mice are initially fed a control diet (Lieber-DeCarli diet *ad libitum*) for 5 days to acclimate them to a liquid diet and tube feeding. After 5 days, EtOH-fed groups are allowed *ad libitum* access to the Lieber-DeCarli diet containing 5% EtOH (vol/vol) for 10 days, while control groups are pair-fed with an isocaloric control diet. In the early morning of day 11, EtOH-fed and pair-fed control mice are provided a single dose of EtOH (5 g/kg body weight) or isocaloric maltose dextrin by gavage. Mice are sacrificed 9 h later, and RNA, protein, and tissue are collected for analysis. This model can be extended for longer periods of chronic feeding (up to 8 weeks) with inclusion of single or multiple EtOH binges. Importantly, in this model, pathogenesis of the intestine and liver are similar to the alternative 3-day binge model (Abdelmegeed et al., 2013), except that the level of CYP2E1 mRNA in the liver was unchanged.

Using the *in vivo* model described above, we prepared whole-cell lysates from whole intestine (included small intestine and colon), liver, and brain isolated from EtOH-fed and pair-fed mice, and we profiled miRNAs and mRNAs differentially expressed in each tissue (Supplementary Tables 2-5). Our miRNA-seq data revealed that 63 mature miRNAs were upregulated more than 2-fold exclusively in the mouse intestine, while 259 miRNAs were downregulated upon EtOH feeding (Fig. 2b and c), which is significantly different from miRNA profiling in rat (Supplementary Fig. 1, Supplementary Tables 6 and 7). Among many miRNAs downregulated in the intestine, we focused on miR-132, miR-212, and miR-378, which are known to target CYP2E1 (Miao et al., 2016; Mohri et al., 2010; Shukla et al., 2013). Cumulative fraction analysis of mRNAs differentially expressed in EtOH-fed intestine revealed that mRNAs targeted by miR-132 and miR-212 are more abundant than the rest of mRNAs (Fig. 2d and Supplementary Table 2), which is unique in the intestine compared to the liver and brain (Supplementary Figs. 2 and 3 and Supplementary Table 2). Levels of other regulatory RNAs, such as circular RNAs, did not fluctuate significantly (Supplementary Figs. 1-3 and Supplementary Table 8). These results demonstrate that there is a correlation between the levels of mRNAs and the miRNAs targeting those mRNAs in the mouse intestine after exposure to EtOH.

A Subset of miRNAs Silences CYP2E1 in T84 and HIEC-6 Human Cell Line

Next, we compared the level of CYP2E1 (immunoblot analysis) and miR-132 (a miRNA known to target CYP2E1; RT-qPCR) in intestine cells isolated from our *in vivo* mouse model (Fig. 3a) and HIEC-6 human cells. Immunoblot analyses showed that CYP2E1 is transiently induced 1 h following the last EtOH gavage (Fig. 3a, top panel), and the CYP2E1-targeting miRNA miR-132 is downregulated immediately after the last EtOH dose (Fig. 3a, bottom panel and Supplementary Fig. 4a). The relative kinetics of up-regulation of CYP2E1 and downregulation of miR-132 support our hypothesis that miRNAs targeting CYP2E1, such as miR-132, regulate CYP2E1 expression in response to EtOH treatment.

Published studies demonstrate that miR-132, miR-212, miR-378, and miR-552 suppress CYP2E1 expression (Miao et al., 2016; Mohri et al., 2010; Shukla et al., 2013). To test this in a cellular model, we overexpressed these miRNAs in human cell lines (T84 and HIEC-6) and compared the relative abundance of CYP2E1 protein and its corresponding mRNA transcripts. Our results demonstrated that the CYP2E1 protein level (Fig. 3b, top panel) is decreased upon overexpression of miR-132, miR-212, or miR-378 (Fig. 3b, bottom panel and Supplementary Fig. 4b), followed by a decrease of *CYP2E1* mRNA (Fig. 3c and Supplementary Fig. 4c). Also, miR-552 overexpression decreased CYP2E1 protein but not transcript levels, suggesting inhibition of *CYP2E1* mRNA translation. Stability of *CYP2E1* mRNA increased upon treatment of EtOH or declined upon overexpression of miR-132 in T84 cells (Fig. 3d). These results revealed that a subset of miRNAs suppress the expression of CYP2E1 in T84 and HIEC-6 human cell line.

MST1 Accelerates Downregulation of Target miRNAs in Intestinal Cells

Our previous studies in yeast demonstrated that *Ste20* mediates phosphorylation of the decapping enzyme 2 (DCP2) in response to oxidative stress (Yoon et al., 2010). We also showed that the ROS-activated human homolog of *Ste20,* MST1, phosphorylates the eukaryotic mRNA translation initiation factor 4E (eIF4E) (Min et al., 2017). MST1 has been shown to interact with the ROS-sensing protein thioredoxin (Chae et al., 2012), and MST1 is activated by ROS signaling. To determine whether MST1 couples EtOH-induced ROS signaling and miRNA-induced CYP2E1 degradation in T84 human cell line, we examined MST1 activation (as measured by MST1 autophosphorylation at T183, or p-MST1) in whole-cell lysates prepared from isolated intestinal crypt cells from EtOH-fed and pair-fed control mice after gavage (Fig. 4a). We found that, following EtOH treatment, MST1 kinase activity was elevated (p-MST1), concomitant with elevated levels of CYP2E1 (Fig. 4a). Our findings support the proposition that MST1 is involved in signaling pathways regulating the expression of CYP2E1 via tight control of miRNA expression.

Next, we followed the protocol from our binge alcohol mouse model in MST1-deficient ($MST1^{-/-}$) mice (Jackson Laboratory) to determine whether MST1 is responsible for EtOH-induced downregulation of miRNAs that target CYP2E1 in the mouse intestine. We first compared the level of miRNAs that target *CYP2E1* mRNA in intestinal crypt cells from EtOH or control-fed $MST1^{+/+}$ mice. As expected, these miRNAs were reduced upon binge EtOH treatment (Fig. 4b). However, binge EtOH treatment did not affect the level of these miRNAs in intestinal crypt cells isolated from $MST1^{-/-}$ animals (Fig. 4b). The observation that

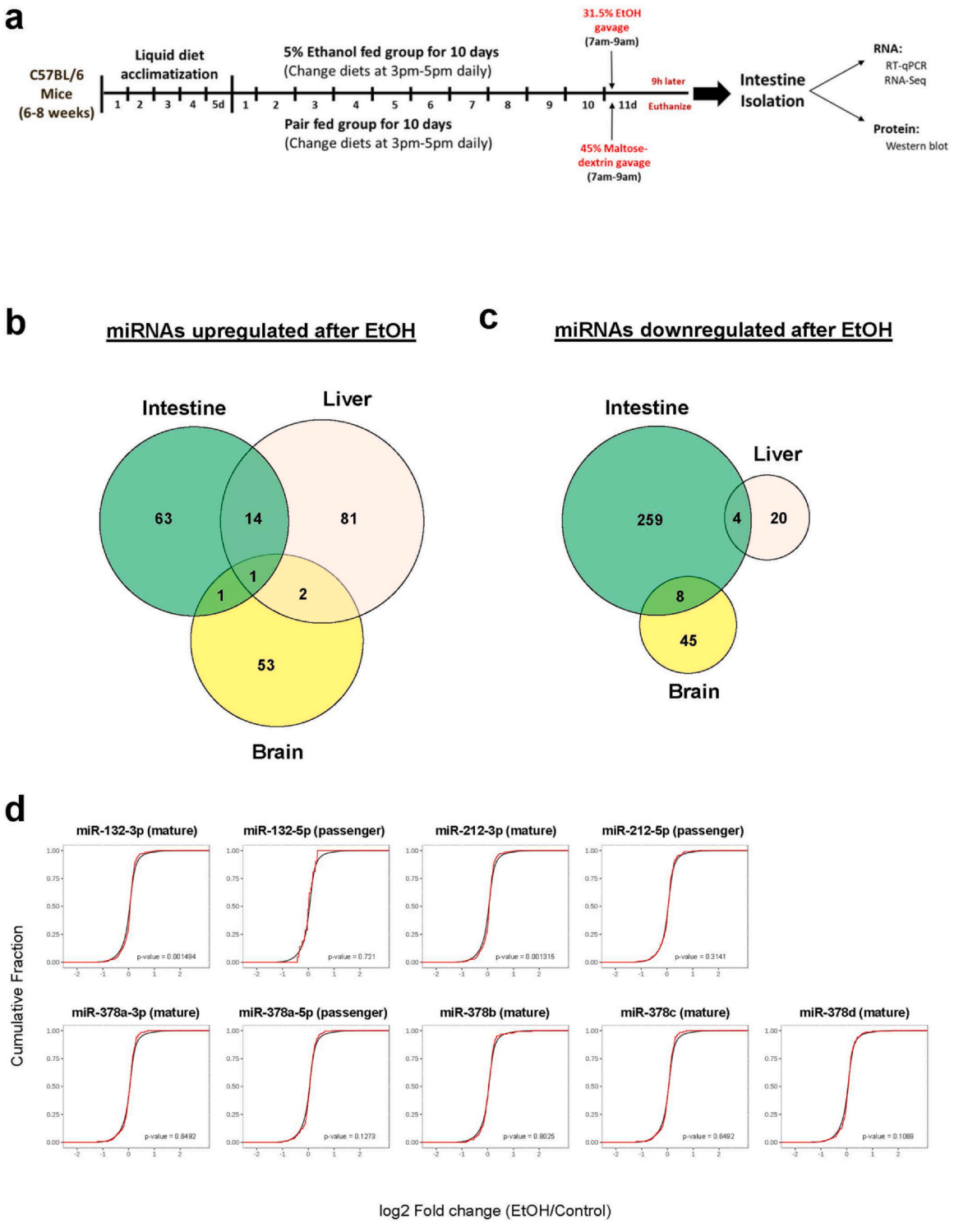

Fig. 2. Profiling of miRNAs and mRNAs in intestine, liver, and brain using a binge alcohol mouse model. (a) Mice were acclimated using a liquid diet (5 days) followed by either EtOH or isocaloric control diets (10 days). Delivery of an EtOH gavage (5 g/kg) on day 11 drives intestinal injury compared to control (maltose dextrin), as determined by RNA, protein, and tissue analysis. (b and c) Number of mature miRNAs overexpressed (2-fold, *B*) or underexpressed (2-fold, *C*) in intestine, liver, or brain upon binge alcohol exposure. (d) Cumulative fraction of mRNA level changes (EtOH/control) in the intestine using a group of mRNAs targeted by miR-132, miR-212, or miR-378 a/b/c/d. Data of miRNA-seq and mRNA-seq are the average of at least 2 independent samples. For statistics of cumulative fraction data, we applied the Kolmogorov-Smirnov test.

MST1 is required for the reduction of miRNAs that influence CYP2E1 levels after binge EtOH treatment implies that MST1 has an important regulatory role in controlling EtOH induction of CYP2E1. Immunoblot analyses confirmed that CYP2E1 is upregulated upon EtOH treatment in control mice and, importantly, that this induction of CYP2E1 is dependent on MST1 (Fig. 4c). Stability of miR-132, miR-212, and miR-378a declined after treatment of EtOH in T84 cells (Fig. 4d). Taken together, these results suggest (1) that MST1 is an integral regulator of CYP2E1 expression in response to binge EtOH treatment and (2) that MST1 acts by promoting degradation of miRNAs that control CYP2E1 levels.

RNA-Binding Protein AUF1 Mediates Downregulation of Target miRNAs in Intestinal Cells

As we previously demonstrated, MST1 is a Ser/Thr kinase that can phosphorylate DCP2 (Yoon et al., 2010) and eIF4E (Min et al., 2017). Moreover, our preliminary data suggested that MST1 modulates the level of miRNAs that target CYP2E1 (Miao et al., 2016; Mohri et al., 2010; Shukla et al., 2013). The RNA-binding protein AUF1, which is known to affect RNA stability, binds these CYP2E1-targeting miRNAs (Yoon et al., 2014, 2015). We therefore reasoned that AUF1 may be a substrate of MST1, and phosphorylation of AUF1 might affect the stability of miRNAs that target CYP2E1. Direct interaction of AUF1 with miR-132 was confirmed by using human RNA-binding domain array. To identify their direct interaction, we utilized a protein array chip immobilized with 354 RNA-binding domains (Chen et al., 2020) for probing with mature miR-132 with 5′-biotin label (Fig. 5a). We isolated 49 RNA-binding proteins (RBPs) directly binding with miR-132 (Fig. 5b, Supplementary Fig. 5, and Supplementary Table 9) and narrowed down heterogeneous nuclear ribonucleoproteins (hnRNP) family proteins, including AUF1 (also called hnRNPD) (Fig. 5c). Reanalysis of the published photoactivatable ribonucleoside-enhanced crosslinking and immunoprecipitation (CLIP) data (GSE21578 and GSE37401) also revealed that AUF1 and the other 9 RBPs directly binds with miR-132 in mammalian cells (Supplementary Fig. 6 and Supplementary Table 10). Direct binding of RBP and mRNA can also influence mRNA translation (Min et al., 2017; Mo et al., 2022). To investigate this possibility, we searched for POSTAR3 to identify RBP-RNA interaction networks containing 1,499 CLIP datasets for 348 RBPs from 10 CLIP-seq techniques (http://111.198.139.65/) (Zhao et al., 2022). Binding site annotations for human CYP2E1 mRNA identified RBPs, such as AGO2, HuR, hnRNPC, CELF2, DIS3L2, NUDT21, and ZC3H7B, interacting with CYP2E1 mRNA. These results show that no AUF1 binding sites were found in CYP2E1 mRNA, suggesting that AUF1 might regulate CYP2E1 mRNA degradation indirectly.

To investigate the connection between AUF1 and MST1, we employed recombinant MST1 and AUF1 proteins and performed an *in vitro* phosphorylation reaction between AUF1 and MST1. Mass spectrometry analysis demonstrated that the MST1-targeted site of phosphorylation on AUF1 resides at Thr127 (Fig. 6a). Importantly, our structural analysis revealed that the Thr127 residue lies within the RNA-binding pocket of AUF1 (Fig. 6b) (Choi et al., 2016). Based on these data, we generated a Thr127 phospho-specific antibody to AUF1 and tested whether AUF1 is phosphorylated in lysates of intestinal crypt cells isolated from control and EtOH-treated $MST1^{+/+}$ and $MST1^{-/-}$ mice. Our immunoblot analysis revealed that phosphorylation of AUF1 at Thr127 (p-AUF1) increased upon EtOH feeding of $MST1^{+/+}$ mice (Fig. 6c). Strikingly, the induction of AUF1 phosphorylation was not detected in intestinal cells isolated from $MST1^{-/-}$ mice. Additionally, knockdown of MST1 in HIEC-6 cells significantly reduced phosphorylation of AUF1 to the same level as inactive AUF1 phosphorylation (Supplementary Fig. 4d). Taken together, these results suggested that, in the intestine, MST1 is the major regulator of AUF1 phosphorylation at Thr127 in response to EtOH treatment.

We next tested the possibility that MST1-mediated phosphorylation affects AUF1 interactions with CYP2E1-targeting miRNAs. We examined the binding of AUF1 to miRNAs that target CYP2E1 in T84 human intestinal cells following overexpression of MST1. Complexes between AUF1 and target miRNAs were identified by immunoprecipitating cell extracts with AUF1 antibodies, followed by RT-qPCR analysis to detect coprecipitated miRNAs. Our analyses revealed that MST1 overexpression significantly reduced the interaction of AUF1 with miR-132, miR-212, and miR-378 (Fig. 6d-f). Immunoblot analysis confirmed that overexpression of HA-tagged MST1 did not affect AUF1 protein levels (Fig. 6g). Furthermore, structural modeling of 3 types of miRNA fragments bound to AUF1 revealed that they fit into the cleft between the 2 RRMs similar to c-fos mRNA, which is one of the targets of HuR (Fig. 6h) (Wang et al., 2013). In addition, the binding modes are like those for miRNA let-7b, a known mature miRNA physically binding to AUF1 (Fig. 6i). These results demonstrated that MST1-mediated AUF1 phosphorylation is critical for the expression of mature miRNAs in human intestinal cells after binge alcohol feeding (Fig. 7).

Intestinal Epithelial Cells Express Nuclear AUF1 and MST1

Since we revealed that the MST1-AUF1-miRNA-CYP2E1 pathway is critical for alcohol-induced intestine injury in our *in vivo* mouse model and our *in vitro* cell model, we asked whether these proteins colocalize in the mouse intestine. To address this question, we collected sections of the intestine from EtOH-fed or pair-fed mice for immunohistochemistry and immunostaining against AUF1. Our immunohistochemistry data showed that AUF1 is expressed in the mouse intestine with intense staining in the crypt area (Supplementary Fig. 7). Immunostaining data identified that AUF1 is predominantly in the nucleus of intestinal cells and colocalize with EPCAM and hepatocyte nuclear factor 4 alpha (Supplementary Figs. 7 and 8). In addition, AUF1 aggregates into granules in a subset of intestinal cells as observed in mammalian cells infected by Coxsackievirus B3 (Wu et al., 2014). EtOH feeding or Cyp2e1 deletion did not affect the expression and localization of AUF1 either (Supplementary Fig. 7). These findings indicated that intestinal AUF1 is expressed in almost crypt area cells and could be involved in intestine injury independent of CYP2E1.

Intestinal Epithelial Stem Cells Are Key Regulators of CYP2E1 Mediated Intestinal Damage

To further investigate mRNA expression of MST1, AUF1, and CYP2E1 in intestinal epithelial cells, we utilized the public single-cell RNA sequencing data generated from C57BL/6J background

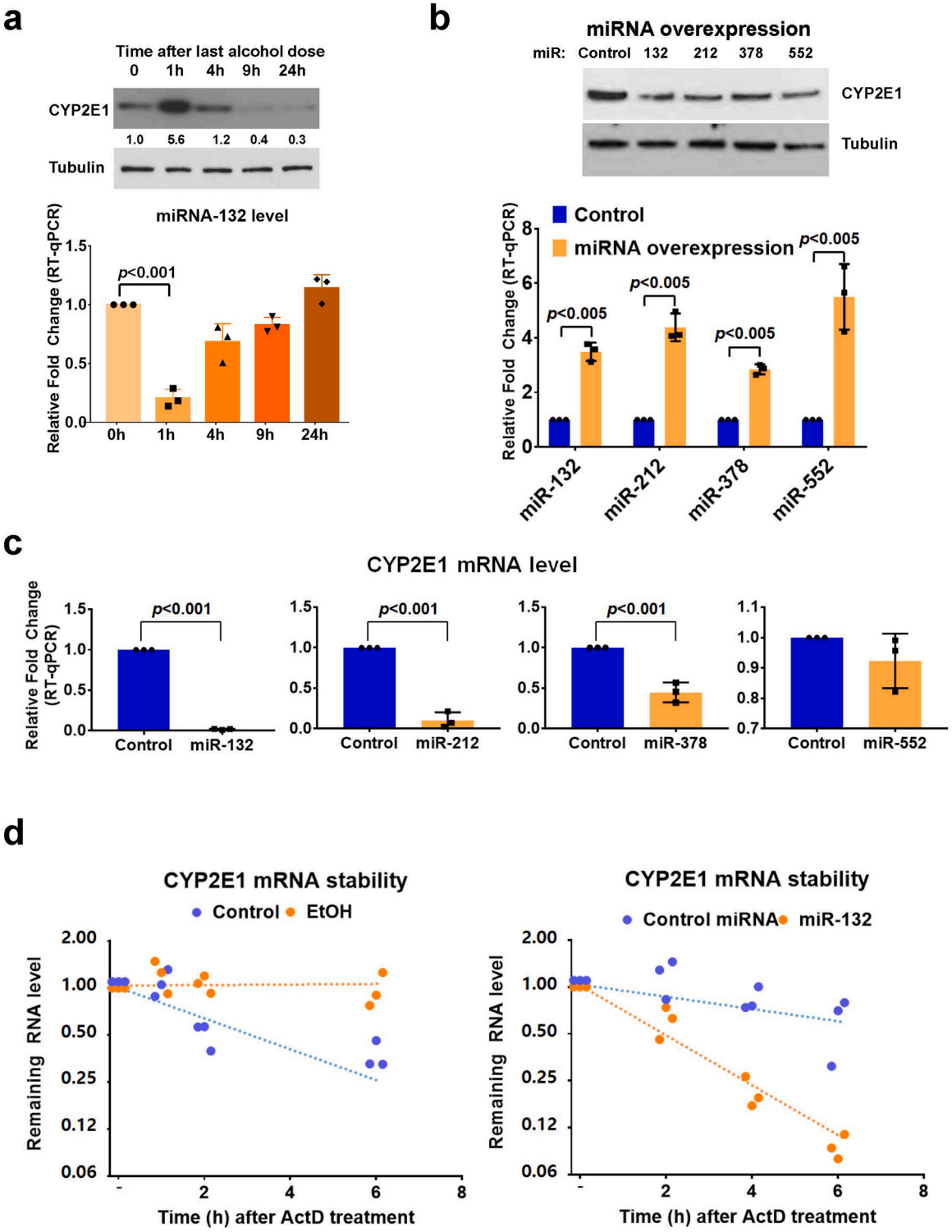

Fig. 3. CYP2E1 is targeted by a subset of miRNAs in mouse and human intestinal cells. (a) Relative expression levels of CYP2E1 (top) and miR-132 (bottom) in isolated mouse intestinal cells at the indicated times post-EtOH treatment. (b) Relative expression level of CYP2E1 protein (top) after overexpression of miR-132, 212, 378, or 552 (bottom) in T84 human intestinal cells. (c) Relative expression level of *CYP2E1* mRNA after overexpression of miRNAs. (d) Stability of *CYP2E1* mRNA calculated from RT-qPCR using RNAs purified from control- or EtOH-treated T84 cells as well as control- or miR-132-transfected cells after exposure to actinomycin D in a given time point. The western blots are representatives of 3 independent experiments. The graphs are the average of 3 independent experiments with standard deviation.

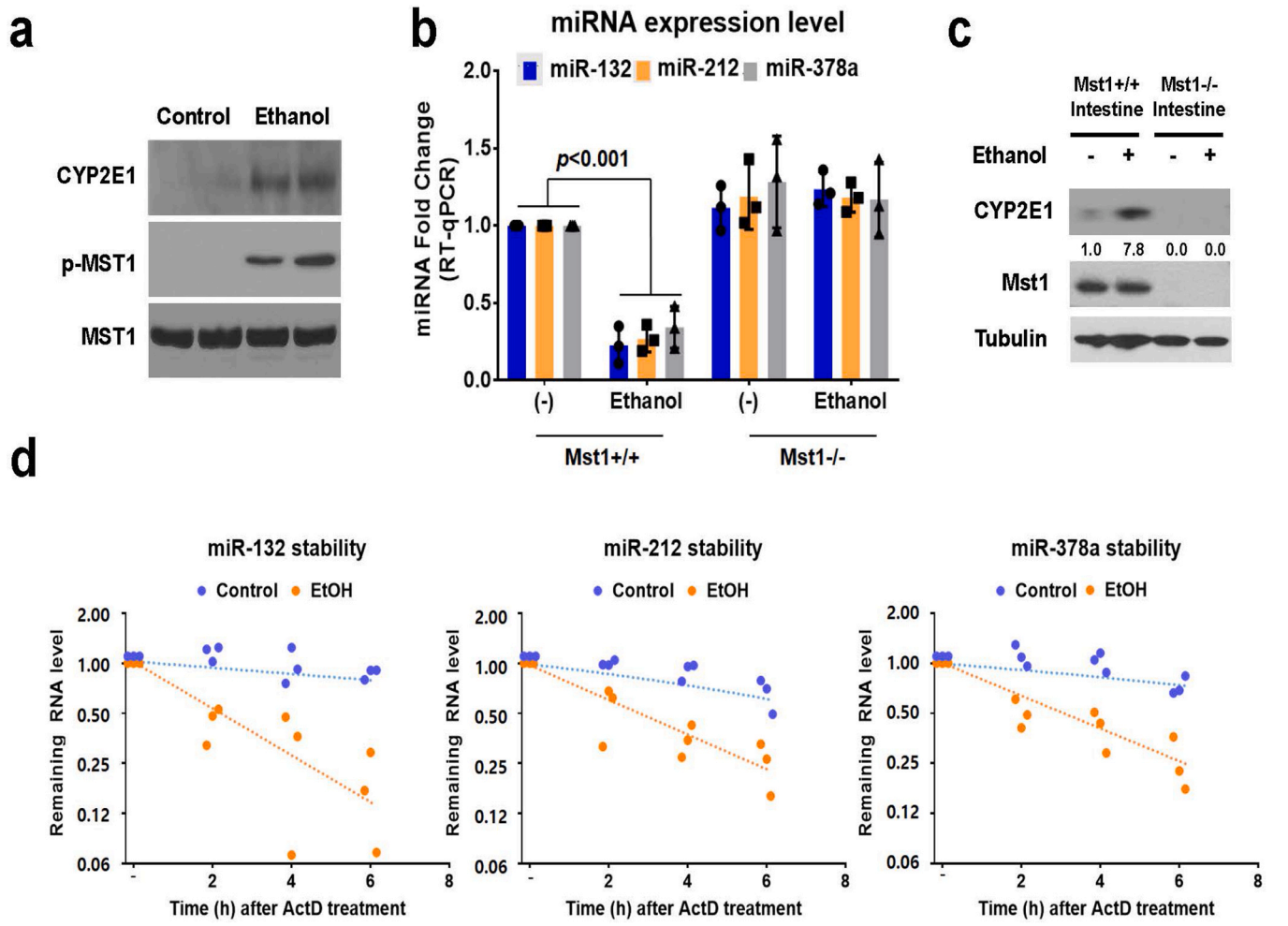

Fig. 4. MST1 in the intestine induces CYP2E1 by AUF1-mediated miRNA downregulation. (a) Western blot analysis of CYP2E1, p-MST1, and MST1 in mouse intestines with or without EtOH feeding. (b) Protein levels of CYP2E1, MST1, and tubulin in intestinal cell lysates from *MST1*$^{+/+}$ and *MST1*$^{-/-}$ mice. (c) Relative expression levels of miR-132, 212, and 378a in intestines of binge EtOH-treated and control *MST1*$^{+/+}$ and *MST1*$^{-/-}$ mice. (d) Stability of miR-132, miR-212, and miR-378a calculated from RT-qPCR using RNAs purified from control- or EtOH-treated T84 cells after exposure to actinomycin D in a given time point. The western blots are representatives of 3 independent experiments. The graphs are the average of 3 independent experiments with standard deviation. MST1, mammalian Ste20-like kinase 1.

mouse colon. Initial analysis clustered and annotated 7 major cell types within the 24 clusters (Supplementary Fig. 9). In accordance with a previous report (Kwon et al., 2021), we initially identified a subset of highly expressed EPCAM, a known marker for intestinal epithelial cells (clusters 0, 1, 5, 6, 7, 9, 10, 12, 13, 14, 16, 17, 18, and 21). Subsequently, we conducted a secondary cluster analysis, resulting in the clustering of intestinal epithelial cells into 16 new clusters (Supplementary Fig. 10a). Among these clusters, we identified intestinal epithelial stem cells expressing high levels of stem cell markers such as *Lgr5*, *Ascl2*, and *Lrig1* (Supplementary Fig. 10b). Additionally, we manually grouped clusters into 4 additional cell types: clusters 0, 1, 2, and 4 as enterocytes; cluster 8 as Paneth cells; clusters 12 and 13 as goblet cells; and clusters 14 and 15 as enteroendocrine cells, based on known markers for intestinal crypt area cell types (Supplementary Fig. 10c) (Yeung et al., 2011).

Transcriptomics studies in human colon organoid models showed a reduction in the stem cell marker LGR5 in intestinal epithelial stem cell types, with a delay or decrease in the cell cycle (Devall et al., 2021). Based on these reports, the expression of AUF1 was concentrated in the intestinal crypt area from the immunofluorescence data of this study (Supplementary Fig. 8), we hypothesized that intestinal epithelinal stem cell express AUF1. To test this hypothesis, we plotted the mean expression values of *Hnrnpd* (AUF1), *Stk4* (MST1), and *Cyp2e1* mRNA of intestinal epithelial cell subclusters. Remarkably, it was observed that the expression levels of *Hnrnpd* and *Elavl1* were significantly elevated in clusters 3 and 5, corresponding to the intestinal epithelial stem cell populations. Moreover, *Stk4* exhibited relatively higher expression levels in these same clusters (clusters 3 and 5). In contrast, expression of *CYP2E1* was found to be very low in almost all clusters (Supplementary Fig. 10d). Additionally, we found that the expression of LGR5 in EtOH-exposed mouse livers was significantly reduced compared to controls (Supplementary Fig. 11). Collectively, these results strongly suggest that the high expression of AUF1 and MST1 in intestinal epithelial stem

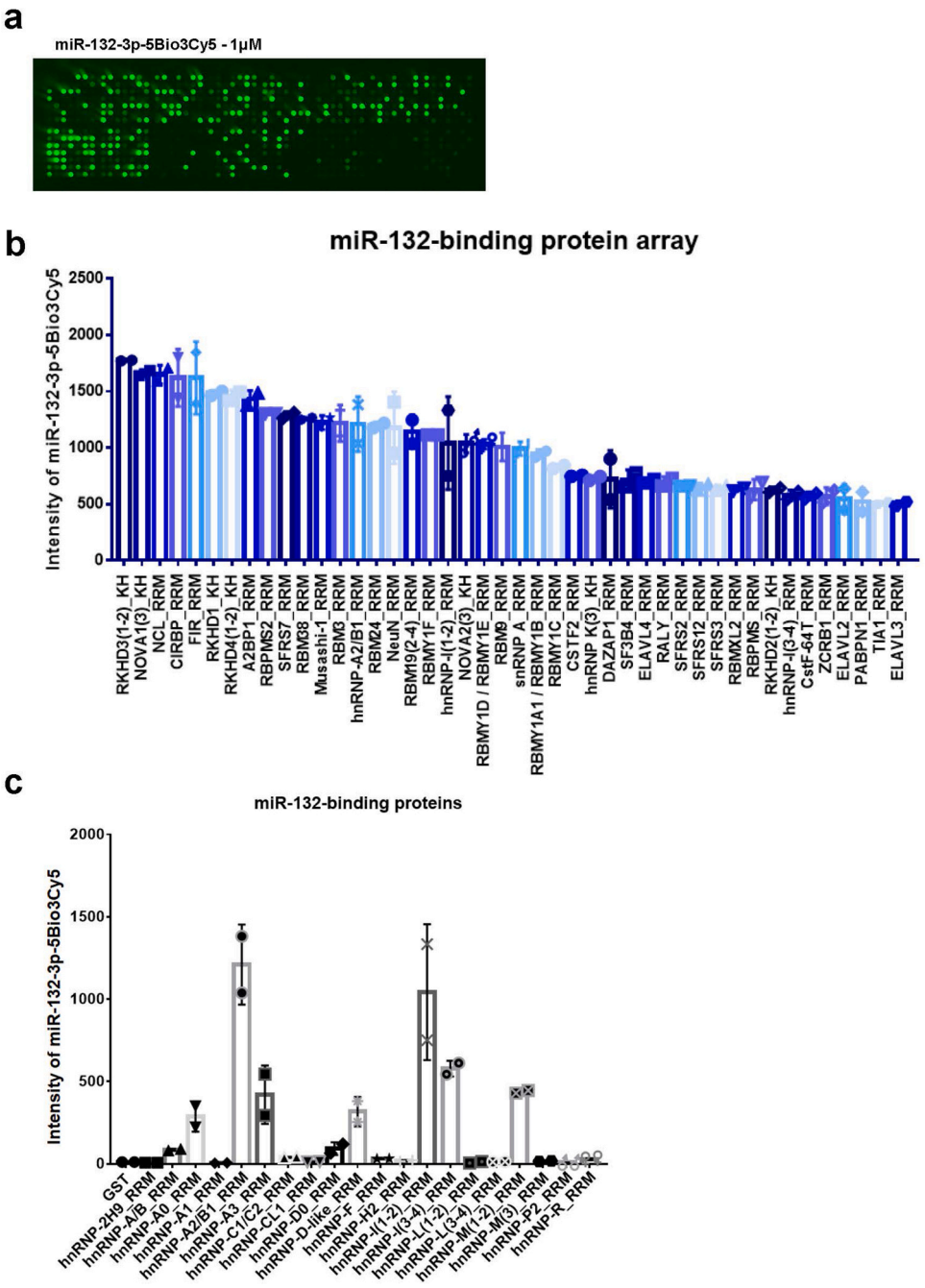

Fig. 5. RNA-binding domain (RBD) array profiled RBPs directly binding with mature miR-132. (a) Fluorescence images of miR-132-3p binding with proteins spotted on the microarray slides. (b and c) Quantification of RBD array intensity of miR-132-3p-5Bio3Cy5 with all RNA-binding domains (*B*) or hnRNPs (*C*).

cells may represent key mechanisms underlying EtOH-mediated intestinal injury.

DISCUSSION

Gut leakage and elevated intestinal permeability to endotoxins have been shown to be regulated by increasing *CYP2E1* mRNA and enhancing CYP2E1 protein levels (Abdelmegeed et al., 2010; Roberts et al., 1994). It has also been shown that miRNAs, including miR-132, miR-212, miR-378, and miR-552, repress the expression of CYP2E1 (Miao et al., 2016; Mohri et al., 2010; Shukla et al., 2013), suggesting these miRNAs contribute to EtOH-induced intestinal injury. In this study, we made 2 key observations that contribute to the molecular mechanisms of how CYP2E1 expression is regulated post-transcriptionally through miRNA-mediated degradation: (1) we demonstrated that the RNA-binding protein AUF1 binds mature miRNAs, and this binding modulates the degradation of target

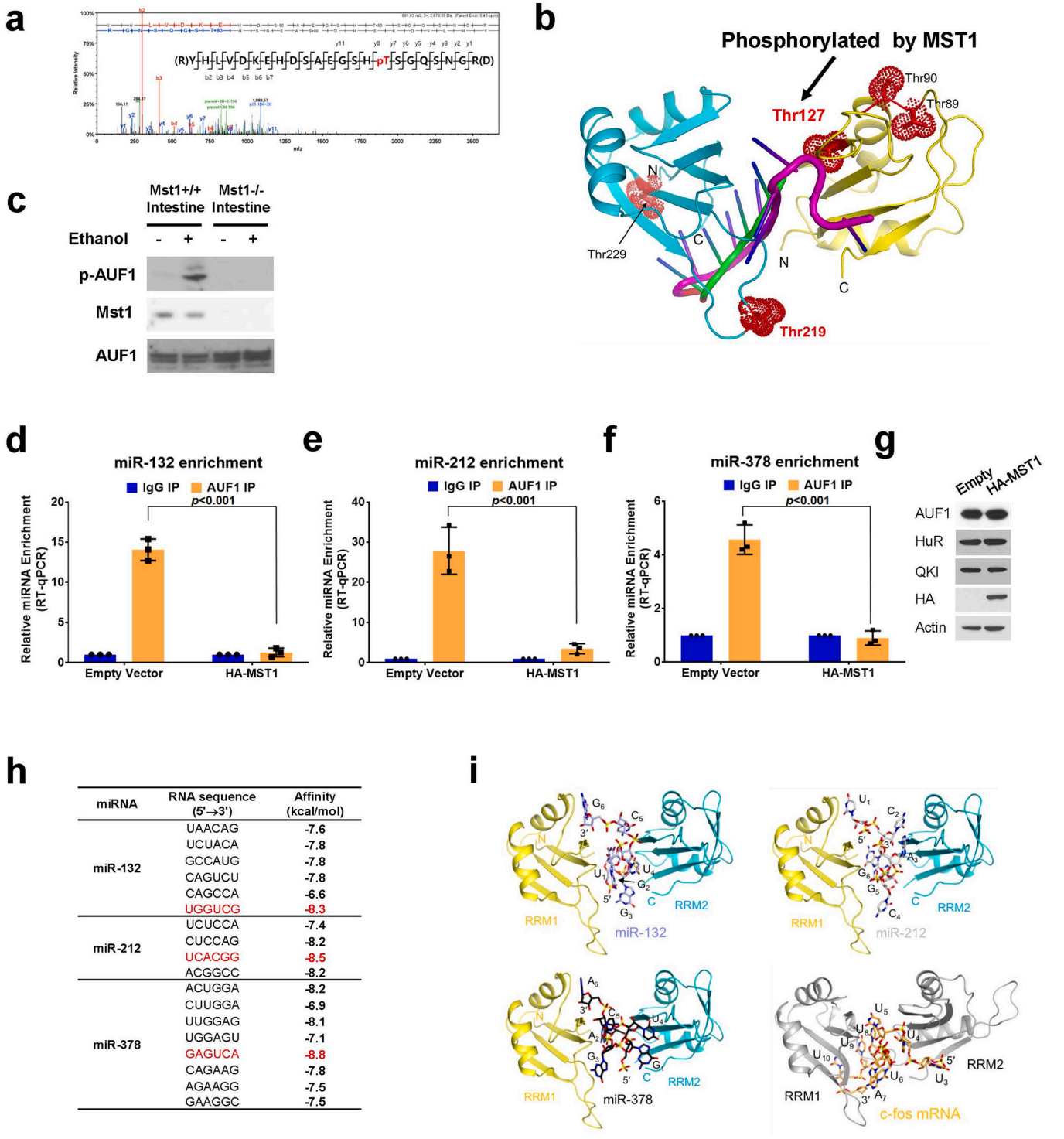

h

miRNA	RNA sequence (5'→3')	Affinity (kcal/mol)
miR-132	UAACAG	-7.6
	UCUACA	-7.8
	GCCAUG	-7.8
	CAGUCU	-7.8
	CAGCCA	-6.6
	UGGUCG	-8.3
miR-212	UCUCCA	-7.4
	CUCCAG	-8.2
	UCACGG	-8.5
	ACGGCC	-8.2
miR-378	ACUGGA	-8.2
	CUUGGA	-6.9
	UUGGAG	-8.1
	UGGAGU	-7.1
	GAGUCA	-8.8
	CAGAAG	-7.8
	AGAAGG	-7.5
	GAAGGC	-7.5

(caption on next page)

Fig. 6. AUF1-mediated miRNA downregulation regulated by phosphorylation of AUF1 by MST1. (a) After performing *in vitro* phosphorylation reaction of MST1 and AUF1, mass spectrometric analysis was performed. Product b- and y-ions are indicated in the peptide sequence (inset) and mass spectrum. (b) Structural model of AUF1 (RRM1 + RRM2) with fragments of 4-bp telomeric DNA (green) and 9 bp *c-fos* mRNA (magenta). The RRM1 and RRM2 of AUF1 are colored in yellow and cyan, respectively. Five Thr residues (space-filling structures in red) phosphorylated by MST1 were identified by MS analysis. (c) Levels of p-AUF1, AUF1, and MST1 in intestinal cell lysates from binge EtOH-treated $MST1^{+/+}$ and $MST1^{-/-}$ mice. (d-f) RT-qPCR levels of miR-132, 212, and 378 in AUF1 immunoprecipitates isolated from T84 human intestinal cells in the presence or absence of MST1 overexpression. (g) Levels of AUF1, HuR, QKI, and actin in T84 cells overexpressing HA-MST1 or transfected with the empty vector. The western blots are representatives of 3 independent experiments. The graphs are the average of 3 independent experiments with standard deviation, SD. (h) Binding energy of 6-bp fragments of each miRNA with AUF1 (RRM1 + RRM2). Fragments of each miRNA showing the best binding energy are highlighted in red color. (i) Structure models of AUF1 in complexes with suited fragments of miR-132, 212, and 378. RRM1 and RRM2 of AUF1 are colored yellow and cyan, respectively. Crystal structure of HuR (gray) in complex with 9-bp fragment of c-fos mRNA is also provided (Pdb code, 4ED5). MST1, mammalian Ste20-like kinase 1.

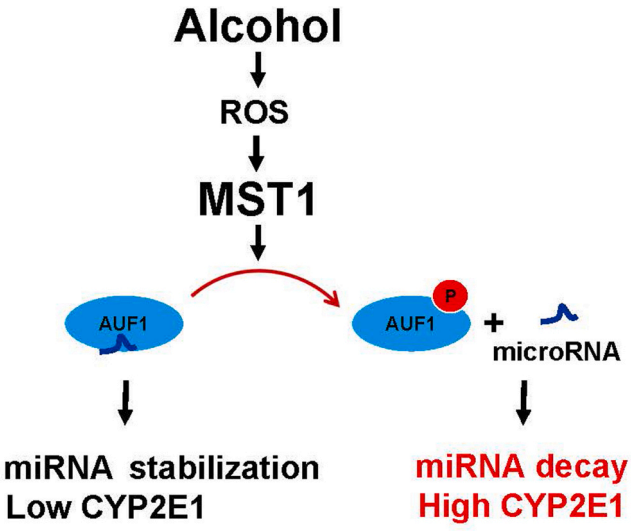

Fig. 7. Proposed model. Molecular mechanisms of how the MST1-AUF1-miRNA-CYP2E1 pathway contributes to alcohol-induced intestinal injury.

mRNAs and (2) we revealed that the yeast homolog of the mammalian MST1 kinase (Ste20) mediates oxidative stress-induced phosphorylation of AUF1. These findings suggest that ROS-mediated signaling modulates AUF1/miRNA interaction through phosphorylation.

MST1/Hippo Pathway in Modulation of Post-Transcriptional Gene Regulation

Our initial analysis revealed that many unique miRNAs were either upregulated or downregulated in tissues from EtOH-fed mice compared to pair-fed mice (Fig. 2). The change in the regulation of miRNAs with the depletion of MST1 suggests that MST1 regulates the expression of these miRNAs and the mRNAs they target. These results support the idea that MST1 regulates mRNA metabolisms through the change in expression of miRNAs as it does for the stabilization of ribosomal mRNAs in yeast (Yoon et al., 2010) and the translation of a long noncoding RNA in human cells (Min et al., 2017). Previously, we identified that MST1 and its homolog regulate the metabolism of mRNAs via direct phosphorylation of DCP2 (Yoon et al., 2010) or eIF4E (Min et al., 2017). Our findings that MST1 phosphorylates a RNA-binding protein, AUF1, for the modulation of miRNA stability and CYP2E1 expression broaden our consensus that MST1 is a critical component of both transcriptional and post-transcriptional gene regulation.

miRNA-Binding Protein AUF1 in Regulation of miRNA and mRNA Stability

Previously, we found that AUF1 binds to the mature miRNA let-7b and promotes let-7b-targeted mRNA decay (Yoon et al., 2014, 2015). In this study, RIP-qPCR analyses revealed that the *CYP2E1*-targeting miRNAs, miR-132, miR-212, and miR-378, also bind to AUF1 (Fig. 6d-g), suggesting that AUF1 regulates CYP2E1 expression through miRNA silencing. Because no structural model is available of AUF1 containing both RRM1 and RRM2, we referred herein to the crystal structure of HuR (RRM1 + RRM2) in a complex with 9-bp fragmented c-fos mRNA (Wang et al., 2013). Based on the outputs from molecular docking among AUF1 and the 6-bp fragmented miRNAs of miR-132, miR-212, and miR-378, we theorized that the miRNAs binding modes of AUF1 could be comparable to those of HuR and c-fos mRNA, as well as to the structural model of AUF1-let-7b miRNA. Furthermore, due to the flexibility of the connecting loop between RRM1 and RRM2, we speculated that conformational changes with certain types of RNA binding could generate enhanced or modulated binding affinities depending on the RNA sequences or secondary structures (Choi et al., 2016).

We also analyzed how EtOH treatment affects the transcripts that are targeted by miR-132, miR-212, and miR-378 using cumulative fraction plots to represent the results (Fig. 2d). We found that EtOH feeding in mice increased the abundance of mRNAs targeted by the miRNAs, since those miRNAs are highly downregulated in intestinal cells isolated from EtOH-fed mice. These results suggested that EtOH-dependent miRNAs play a significant role in the abundance of mRNAs targeted by the miRNAs, possibly through an increase in miRNA stability. Additionally, because the target mRNAs are controlled by the action of miRNAs, we concluded that RNA-biding proteins directly interacting with these miRNAs are likely to control miRNA stability in intestinal cells (Min et al., 2017; Yoon et al., 2015; Zealy et al., 2017).

RBP and Noncoding RNA Interaction in mRNA Translation Regulation

Our RNA-binding domain arrays have identified various RBP domains that directly bind to miR-132 (Fig. 5a-c). This is noteworthy, as a single miRNA can potentially target approximately 200

transcripts due to its simple structure and short structural characteristics (Krek et al., 2005). The implications of this multitarget effect have the potential to significantly increase the complexity of the noncoding RNAs' roles, which encompasses interactions.

The mechanisms that may affect AUF1/miRNA-mediated mRNA regulation could be influenced by several factors, including the presence of miRNA binding by other RNA-binding proteins following miRNA maturation, the presence of arthrobacter luteus repeats and binding sites in long noncoding RNAs, as well as the sponge effects through competing endogenous RNAs (include lncRNA). Previous results have shown that RBP HuR destabilizes lincRNA-p21 and improves mRNA translation by binding to Ago2/let7-b (Yoon et al., 2012) and AUF1 facilitated microRNA transfer to AGO2 (Yoon et al., 2015). In conjunction with these findings, the miRNA reverse transcription quantitative PCR (RT-qPCR) results (Fig. 3b and c, Supplementary Fig. 4b and c) demonstrated that direct binding of AUF1 was not observed in the POSTAR3 database, demonstrated that its regulation likely occurs indirectly via stabilization of miRNA.

In the case of lncRNAs, recent research has indicated that the downregulation of lncRNA Linc00844, following acetaminophen treatment, plays a crucial role in regulating the expression of the drug-metabolizing enzyme CYP2E1 mRNA and protein in human cells (Li et al., 2020). In addition, the presence of lncRNA partial complementary sequences for human and mouse CYP2E1 indicates the potential contribution of noncoding RNAs to the regulation mRNA stability and/or translation (Supplementary Tables 11 and 12). Taken together, at least a few noncoding RNAs regulated by RBP and the translational regulation and decay kinetics of the target mRNAs they regulate may be involved in alcohol-induced intestinal injury and recovery mechanisms (Xiao et al., 2019; Zou et al., 2016). However, follow-up studies are necessary to confirm other miRNAs and lncRNAs interacting with AUF1, especially in the context of alcohol binge drinking.

MST1-Auf1-miRNA-Cyp2e1 Signaling Cascade Controlling Alcohol-Induced Gut Injury

Because our experiments revealed that MST1 influences the expression of CYP2E1 and miRNAs in response to alcohol consumption, our results suggested that an MST1 or CYP2E1 inhibitor (Anand et al., 2009; Fan et al., 2016; Gebhardt et al., 1997; Ron and Messing, 2013) could be used to treat patients with AUD. There are various ways we can expand on the results of our findings. First, more CYP2E1 genes could be similarly screened for miR-132, miR-212, and miR-378, whose regulation controls alcohol-induced gut injury. Second, the miRNAs we examined in the study could be used to screen for alcohol-induced injury of gut, liver, and brain, in which miRNAs may play a critical role. Third, trials in the mice model are needed to verify the importance of the pathway, MST1-AUF1-miRNA-Cyp2e1, in cell models (Fig. 7). Fourth, to verify the findings in our experiments, more miRNAs could be screened for their impact on miRNA expression and on target mRNA regulation. Altogether, findings from our current study have experimental and clinical significance in the post-transcriptional regulation of alcohol-induced gut injury.

FUNDING AND SUPPORT

J.-H.J., S.K., and J.-H.Y. were supported by R01AA027532. H.M., J.-H.J., and J.-H.Y. were supported by a startup fund from the University of Oklahoma. Y.L.C. and J.J. were supported by the National Research Foundation of Korea 2018R1D1A1B07040282, P.Z. and S.S were supported by Integrative Morphology Core of the Digestive Diseases Research Core Center in Cincinnati P30 DK078392, C.A.S. and M.T.B. were supported by the GM126421 and RP180804. J.H.C was supported by NRF-2022R1F1A1073775. Y.-K.K. was supported by National Research Foundation of Korea 2021R1A2B5B02001501. S.C. and J.K. were supported by Brain Korea 21 FOUR Project for Medical Science, Chungnam National University.

AUTHOR CONTRIBUTIONS

The research was conceived and designed by J.-H.Y., J.H.C, J.J, and J.K. Most of the experiments were performed by H.M., S.L, S.C, J.-H.J., S.K., Y.L.C, B.D., C.T.Y., A.B., J.P., and L.N. P.Z. and S.S performed immunohistochemistry and immunofluorescence assays. Y.-K.K. performed circular RNA analysis. D.-C.K. and J.H.C performed structural analyses of AUF1 and miRNAs. C.A.S. and M.T.B. performed RNA-binding domain analysis.

DECLARATION OF COMPETING INTERESTS

The authors declare no competing interests.

DATA AVAILABILITY STATEMENT

RNA-Seq data are available in the gene expression omnibus (GEO) database under accession number GSE206348. The scRNA-seq data used in this study were downloaded from GEO public data repositories, accessible number is GSE163638.

ACKNOWLEDGMENTS

We thank Dr B.J. Song in the National Institute on Alcohol Abuse and Alcoholism-Intramural Research Program for providing mouse and rat tissues for miRNA and mRNA profiling and immunohistochemistry. We thank Dr J.-I. Park in the MD Anderson Cancer Center for providing technical comments on intestine organoid culture.

APPENDIX A. SUPPLEMENTAL MATERIAL

Supplemental material associated with this article can be found online at: doi:10.1016/j.mocell.2024.100074.

ORCID

Sungyul Lee https://orcid.org/0000-0003-3207-1199
Suyoung Choi https://orcid.org/0000-0002-7474-610X
Ji-Hoon Jeong https://orcid.org/0000-0002-2404-6850
Seungbeom Ko https://orcid.org/0000-0002-8457-3134
Soona Shin https://orcid.org/0000-0001-5696-9505
Dong-Chan Kim https://orcid.org/0000-0002-9361-8023
Cari A. Sagum https://orcid.org/0000-0001-6101-7162
Mark T. Bedford https://orcid.org/0000-0002-8899-1050
Young-Kook Kim https://orcid.org/0000-0001-6434-2235
Jaeyul Kwon https://orcid.org/0000-0002-2452-4111
Je-Hyun Yoon https://orcid.org/0000-0001-7615-8654

Received May 21, 2024
Accepted May 24, 2024
Available online 18 June 2024.

REFERENCES

Abdelmegeed, M.A., Banerjee, A., Jang, S., Yoo, S.H., Yun, J.W., Gonzalez, F.J., Keshavarzian, A., and Song, B.J. (2013). CYP2E1 potentiates binge alcohol-induced gut leakiness, steatohepatitis, and apoptosis. Free Radic. Biol. Med. *65*, 1238-1245.

Abdelmegeed, M.A., Moon, K.H., Chen, C., Gonzalez, F.J., and Song, B.J. (2010). Role of cytochrome P450 2E1 in protein nitration and ubiquitin-mediated degradation during acetaminophen toxicity. Biochem. Pharmacol. *79*, 57-66.

Anand, R., Maksimoska, J., Pagano, N., Wong, E.Y., Gimotty, P.A., Diamond, S.L., Meggers, E., and Marmorstein, R. (2009). Toward the development of a potent and selective organoruthenium mammalian sterile 20 kinase inhibitor. J. Med. Chem. *52*, 1602-1611.

Banerjee, A., Abdelmegeed, M.A., Jang, S., and Song, B.J. (2015). Increased sensitivity to binge alcohol-induced gut leakiness and inflammatory liver disease in HIV transgenic rats. PLoS One, *10*, Article e0140498.

Bertola, A., Mathews, S., Ki, S.H., Wang, H., and Gao, B. (2013). Mouse model of chronic and binge ethanol feeding (the NIAAA model). Nat. Protoc. *8*, 627-637.

Bolger, A.M., Lohse, M., and Usadel, B. (2014). Trimmomatic: a flexible trimmer for Illumina sequence data. Bioinformatics, *30*, 2114-2120.

Chae, J.S., Gil Hwang, S., Lim, D.S., and Choi, E.J. (2012). Thioredoxin-1 functions as a molecular switch regulating the oxidative stress-induced activation of MST1. Free Radic. Biol. Med. *53*, 2335-2343.

Chen, J., Sagum, C., and Bedford, M.T. (2020). Protein domain microarrays as a platform to decipher signaling pathways and the histone code. Methods, *184*, 4-12.

Chen, Y.Y., Zhang, C.L., Zhao, X.L., Xie, K.Q., and Zeng, T. (2014). Inhibition of cytochrome P4502E1 by chlormethiazole attenuated acute ethanol-induced fatty liver. Chem. Biol. Interact. *222*, 18-26.

Cheng, J., Metge, F., and Dieterich, C. (2016). Specific identification and quantification of circular RNAs from sequencing data. Bioinformatics, *32*, 1094-1096.

Cho, Y.E., Mezey, E., Hardwick, J.P., Salem, N., Jr., Clemens, D.L., and Song, B.J. (2017). Increased ethanol-inducible cytochrome P450-2E1 and cytochrome P450 isoforms in exosomes of alcohol-exposed rodents and patients with alcoholism through oxidative and endoplasmic reticulum stress. Hepatol. Commun. *1*, 675-690.

Choi, Y.J., Yoon, J.H., and Chang, J.H. (2016). Crystal structure of the N-terminal RNA recognition motif of mRNA decay regulator AUF1. Biomed. Res. Int.Article 3286191.

Devall, M., Jennelle, L.T., Bryant, J., Bien, S., Peters, U., Powell, S., and Casey, G. (2020). Modeling the effect of prolonged ethanol exposure on global gene expression and chromatin accessibility in normal 3D colon organoids. PLoS One, *15*, Article e0227116.

Devall, M., Plummer, S.J., Bryant, J., Jennelle, L.T., Eaton, S., Dampier, C.H., Huyghe, J.R., Peters, U., Powell, S.M., and Casey, G. (2021). Ethanol exposure drives colon location specific cell composition changes in a normal colon crypt 3D organoid model. Sci. Rep. *11*, 432.

Enokizono, Y., Konishi, Y., Nagata, K., Ouhashi, K., Uesugi, S., Ishikawa, F., and Katahira, M. (2005). Structure of hnRNP D complexed with single-stranded telomere DNA and unfolding of the quadruplex by heterogeneous nuclear ribonucleoprotein D. J. Biol. Chem. *280*, 18862-18870.

Fan, F., He, Z., Kong, L.L., Chen, Q., Yuan, Q., Zhang, S., Ye, J., Liu, H., Sun, X., Geng, J., et al. (2016). Pharmacological targeting of kinases MST1 and MST2 augments tissue repair and regeneration. Sci. Transl. Med. *8*, Article 352ra108.

Forsyth, C.B., Tang, Y., Shaikh, M., Zhang, L., and Keshavarzian, A. (2010). Alcohol stimulates activation of Snail, epidermal growth factor receptor signaling, and biomarkers of epithelial-mesenchymal transition in colon and breast cancer cells. Alcohol Clin. Exp. Res. *34*, 19-31.

Gebhardt, A.C., Lucas, D., Menez, J.F., and Seitz, H.K. (1997). Chlormethiazole inhibition of cytochrome P450 2E1 as assessed by chlorzoxazone hydroxylation in humans. Hepatology, *26*, 957-961.

Kim, Y.K. (2019). Analysis of circular RNAs in the coronary arteries of patients with Kawasaki disease. J. Lipid Atheroscler. *8*, 50-57.

Krek, A., Grun, D., Poy, M.N., Wolf, R., Rosenberg, L., Epstein, E.J., MacMenamin, P., da Piedade, I., Gunsalus, K.C., Stoffel, M., et al. (2005). Combinatorial microRNA target predictions. Nat. Genet. *37*, 495-500.

Kwon, O., Jung, K.B., Lee, K.R., Son, Y.S., Lee, H., Kim, J.J., Kim, K., Lee, S., Song, Y.K., Jung, J., et al. (2021). The development of a functional human small intestinal epithelium model for drug absorption. Sci. Adv. *7*, 1-17.

Lee, S., Zhou, P., Gupta, A., and Shin, S. (2018). Reactive ductules are associated with angiogenesis and tumor cell proliferation in pediatric liver cancer. Hepatol. Commun. *2*, 1199-1212.

Li, D., Wu, L., Knox, B., Chen, S., Tolleson, W.H., Liu, F., Yu, D., Guo, L., Tong, W., and Ning, B. (2020). Long noncoding RNA LINC00844-mediated molecular network regulates expression of drug metabolizing enzymes and nuclear receptors in human liver cells. Arch. Toxicol. *94*, 1637-1653.

Lu, R., Voigt, R.M., Zhang, Y., Kato, I., Xia, Y., Forsyth, C.B., Keshavarzian, A., and Sun, J. (2017). Alcohol injury damages intestinal stem cells. Alcohol Clin. Exp. Res. *41*, 727-734.

Miao, L., Yao, H., Li, C., Pu, M., Yao, X., Yang, H., Qi, X., Ren, J., and Wang, Y. (2016). A dual inhibition: microRNA-552 suppresses both transcription and translation of cytochrome P450 2E1. Biochim. Biophys. Acta, *1859*, 650-662.

Min, K.W., Davila, S., Zealy, R.W., Lloyd, L.T., Lee, I.Y., Lee, R., Roh, K.H., Jung, A., Jemielity, J., Choi, E.J., et al. (2017a). eIF4E phosphorylation by MST1 reduces translation of a subset of mRNAs, but increases lncRNA translation. Biochim. Biophys. Acta Gene. Regul. Mech. *1860*, 761-772.

Min, K.W., Jo, M.H., Shin, S., Davila, S., Zealy, R.W., Kang, S.I., Lloyd, L.T., Hohng, S., and Yoon, J.H. (2017). AUF1 facilitates microRNA-mediated gene silencing. Nucleic Acids Res. *45*, 6064-6073.

Miyoshi, H., and Stappenbeck, T.S. (2013). In vitro expansion and genetic modification of gastrointestinal stem cells in spheroid culture. Nat. Protoc. *8*, 2471-2482.

Mo, L., Meng, L., Huang, Z., Yi, L., Yang, N., and Li, G. (2022). An analysis of the role of HnRNP C dysregulation in cancers. Biomark. Res. *10*, 19.

Mohri, T., Nakajima, M., Fukami, T., Takamiya, M., Aoki, Y., and Yokoi, T. (2010). Human CYP2E1 is regulated by miR-378. Biochem. Pharmacol. *79*, 1045-1052.

Natarajan, S.K., Pachunka, J.M., and Mott, J.L. (2015). Role of microRNAs in alcohol-induced multi-organ injury. Biomolecules, *5*, 3309-3338.

Newton, D.J., Wang, R.W., and Lu, A.Y. (1995). Cytochrome P450 inhibitors. Evaluation of specificities in the in vitrometabolism of therapeutic agents by human liver microsomes. Drug Metab. Dispos. *23*, 154-158.

O'Boyle, N.M., Banck, M., James, C.A., Morley, C., Vandermeersch, T., and Hutchison, G.R. (2011). Open Babel: an open chemical toolbox. J. Cheminform. *3*, 33.

Parigi, S.M., Larsson, L., Das, S., Ramirez Flores, R.O., Frede, A., Tripathi, K.P., Diaz, O.E., Selin, K., Morales, R.A., Luo, X., et al. (2022). The spatial transcriptomic landscape of the healing mouse intestine following damage. Nat. Commun. *13*, 828.

Reuben, A. (2008). Alcohol and the liver. Curr. Opin. Gastroenterol. *24*, 328-338.

Roberts, B.J., Shoaf, S.E., Jeong, K.S., and Song, B.J. (1994). Induction of CYP2E1 in liver, kidney, brain and intestine during chronic ethanol administration and withdrawal: evidence that CYP2E1 possesses a rapid phase half-life of 6 h or less. Biochem. Biophys. Res. Commun. *205*, 1064-1071.

Ron, D., and Messing, R.O. (2013). Signaling pathways mediating alcohol effects. Curr. Top. Behav. Neurosci. *13*, 87-126.

Sacks, J.J., Gonzales, K.R., Bouchery, E.E., Tomedi, L.E., and Brewer, R.D. (2015). 2010 national and state costs of excessive alcohol consumption. Am. J. Prev. Med. *49*, e73-e79.

Sheron, N. (2016). Alcohol and liver disease in Europe–simple measures have the potential to prevent tens of thousands of premature deaths. J. Hepatol. *64*, 957-967.

Shukla, U., Tumma, N., Gratsch, T., Dombkowski, A., and Novak, R.F. (2013). Insights into insulin-mediated regulation of CYP2E1: miR-132/-212 targeting of CYP2E1 and role of phosphatidylinositol 3-kinase, Akt (protein kinase B), mammalian target of rapamycin signaling in regulating miR-132/-212 and miR-122/-181a expression in primary cultured rat hepatocytes. Drug Metab. Dispos. *41*, 1769-1777.

Stahre, M., Roeber, J., Kanny, D., Brewer, R.D., and Zhang, X. (2014). Contribution of excessive alcohol consumption to deaths and years of potential life lost in the United States. Prev. Chronic Dis. *11*, Article E109.

Stresser, D.M., Perloff, E.S., Mason, A.K., Blanchard, A.P., Dehal, S.S., Creegan, T.P., Singh, R., and Gangl, E.T. (2016). Selective time- and NADPH-dependent inhibition of human CYP2E1 by clomethiazole. Drug Metab. Dispos, *44*, 1424-1430.

Suh, H.N., Kim, M.J., Jung, Y.S., Lien, E.M., Jun, S., and Park, J.I. (2017). Quiescence exit of Tert(+) stem cells by Wnt/beta-catenin is indispensable for intestinal regeneration. Cell Rep. *21*, 2571-2584.

Trott, O., and Olson, A.J. (2010). AutoDock Vina: improving the speed and accuracy of docking with a new scoring function, efficient optimization, and multithreading. J. Comput. Chem. *31*, 455-461.

Wang, H., Zeng, F., Liu, Q., Liu, H., Liu, Z., Niu, L., Teng, M., and Li, X. (2013). The structure of the ARE-binding domains of Hu antigen R (HuR) undergoes conformational changes during RNA binding. Acta Crystallogr. D Biol. Crystallogr. *69*, 373-380.

Wang, H., Zeng, F., Liu, Q., Liu, H., Liu, Z., Niu, L., Teng, M., and Li, X. (2013). The structure of the ARE-binding domains of Hu antigen R (HuR) undergoes conformational changes during RNA binding. Acta Crystallogr. D Biol. Crystallogr. *69*, 373-380.

Wepf, A., Glatter, T., Schmidt, A., Aebersold, R., and Gstaiger, M. (2009). Quantitative interaction proteomics using mass spectrometry. Nat. Methods, *6*, 203-205.

Wu, S., Lin, L., Zhao, W., Li, X., Wang, Y., Si, X., Wang, T., Wu, H., Zhai, X., Zhong, X., et al. (2014). AUF1 is recruited to the stress granules induced by coxsackievirus B3. Virus Res. *192*, 52-61.

Xiao, L., Gorospe, M., and Wang, J.Y. (2019). Long noncoding RNAs in intestinal epithelium homeostasis. Am. J. Physiol. Cell Physiol. *317*, C93-C100.

Yeung, T.M., Chia, L.A., Kosinski, C.M., and Kuo, C.J. (2011). Regulation of self-renewal and differentiation by the intestinal stem cell niche. Cell. Mol. Life Sci. *68*, 2513-2523.

Yoon, J.H., Abdelmohsen, K., Srikantan, S., Yang, X., Martindale, J.L., De, S., Huarte, M., Zhan, M., Becker, K.G., and Gorospe, M. (2012). LincRNA-p21 suppresses target mRNA translation. Mol. Cell. *47*, 648-655.

Yoon, J.H., Choi, E.J., and Parker, R. (2010). Dcp2 phosphorylation by Ste20 modulates stress granule assembly and mRNA decay in Saccharomyces cerevisiae. J. Cell. Biol. *189*, 813-827.

Yoon, J.H., De, S., Srikantan, S., Abdelmohsen, K., Grammatikakis, I., Kim, J., Kim, K.M., Noh, J.H., White, E.J., Martindale, J.L., et al. (2014). PAR-CLIP analysis uncovers AUF1 impact on target RNA fate and genome integrity. Nat. Commun. *5*, 5248.

Yoon, J.H., Jo, M.H., White, E.J., De, S., Hafner, M., Zucconi, B.E., Abdelmohsen, K., Martindale, J.L., Yang, X., Wood, W.H., 3rd, et al. (2015). AUF1 promotes let-7b loading on Argonaute 2. Genes Dev. *29*, 1599-1604.

Yoon Y.H. (2010). Liver cirrhosis mortality in the United States, 1970–2007. U.S. Department of Health and Human Services, Public Health Service, National Institutes of Health.

Yun, H.J., Yoon, J.H., Lee, J.K., Noh, K.T., Yoon, K.W., Oh, S.P., Oh, H.J., Chae, J.S., Hwang, S.G., Kim, E.H., et al. (2011). Daxx mediates activation-induced cell death in microglia by triggering MST1 signalling. EMBO J. *30*, 2465-2476.

Zealy, R.W., Wrenn, S.P., Davila, S., Min, K.W., and Yoon, J.H. (2017). microRNA-binding proteins: specificity and function. Wiley Interdiscip. Rev .RNA, *8*, 1-8.

Zhao, W., Zhang, S., Zhu, Y., Xi, X., Bao, P., Ma, Z., Kapral, T.H., Chen, S., Zagrovic, B., Yang, Y.T., Lu, Z.J., et al. (2022). POSTAR3: an updated platform for exploring post-transcriptional regulation coordinated by RNA-binding proteins. Nucleic Acids Res. *50*, D287-D294.

Zou, T., Jaladanki, S.K., Liu, L., Xiao, L., Chung, H.K., Wang, J.Y., Xu, Y., Gorospe, M., and Wang, J.Y. (2016). H19 long noncoding RNA regulates intestinal epithelial barrier function via MicroRNA 675 by interacting with RNA-binding protein HuR. Mol. Cell. Biol. *36*, 1332-1341.